PNAS RESEARCH ARTICLE | APPLIED PHYSICAL SCIENCES ENVIRONMENTAL SCIENCES

Assessing suspension and infectivity times of virus-loaded aerosols involved in airborne transmission

Tania Merhi[a], Omer Atasi[a], Clémence Coetsier[a], Benjamin Lalanne[a], and Kevin Roger[a,1]

Edited by David Weitz, Harvard University, Cambridge, MA; received March 18, 2022; accepted June 29, 2022

Airborne transmission occurs through droplet-mediated transport of viruses following the expulsion of an aerosol by an infected host. Transmission efficiency results from the interplay between virus survival in the drying droplet and droplet suspension time in the air, controlled by the coupling between water evaporation and droplet sedimentation. Furthermore, droplets are made of a respiratory fluid and thus, display a complex composition consisting of water and nonvolatile solutes. Here, we quantify the impact of this complex composition on the different phenomena underlying transmission. Solutes lead to a nonideal thermodynamic behavior, which sets an equilibrium droplet size that is independent of relative humidity. In contrast, solutes do not significantly hinder transport due to their low initial concentration. Realistic suspension times are computed and increase with increasing relative humidity or decreasing temperature. By uncoupling drying and suspended stages, we observe that enveloped viruses may remain infectious for hours in dried droplets. However, their infectivity decreases with increasing relative humidity or temperature after dozens of minutes. Examining expelled droplet size distributions in the light of these results leads to distinguishing two aerosols. Most droplets measure between 0 and 40 μm and compose an aerosol that remains suspended for hours. Its transmission efficiency is controlled by infectivity, which decreases with increasing humidity and temperature. Larger droplets form an aerosol that only remains suspended for minutes but corresponds to a much larger volume and thus, viral load. Its transmission efficiency is controlled by droplet suspension time, which decreases with increasing humidity and decreasing temperature.

aerosol | evaporation | virus | infectivity | saliva

Significance

Respiratory viruses are carried by droplets containing not only water but also, proteins and salts. This research investigates the impact of fluid complexity, air humidity, and temperature on the two characteristic times underlying airborne transmission, which assess how long droplets remain suspended in air and how long viruses survive in these dried droplets. Combining the quantitative assessment of these times with the exhaled droplets' size distribution highlights two distinct aerosols, displaying a different environmental dependence of their transmission efficiency. The first aerosol contains small droplets, which are more numerous and remain suspended for hours. The second aerosol contains larger droplets that can only remain suspended for minutes but represent a much higher volume and consequently, a higher viral load.

Airborne transmission of viruses has been under intense and renewed scrutiny in the context of the COVID-19 pandemic (1–10). As we speak, sing, cough, or sneeze, we indeed emit droplets of respiratory fluids suspended in air (11–13), an aerosol, which can transport viruses to another individual. Assessing transmission efficiency thus requires a comprehensive description of droplet drying and sedimentation processes, which control the aerosol suspension time, together with an evaluation of virus survival at low water concentration for a diversity of initial sizes, compositions, and environmental conditions, such as humidity and temperature. The challenge stems from the juxtaposition of several elements of complexity, notably the coupling between different nonequilibrium processes and the multicomponent nature of respiratory fluids.

While droplet generation was already a topic a century ago during the Spanish influenza pandemic (14), several recent works have investigated anew this problem with contemporary techniques and measured the relationship between droplet size and generation mechanism (11–13, 15–18). Three emission modes have been identified, and the resulting droplet sizes were characterized by Johnson et al. (17). Bronchiolar and laryngeal modes yield droplet distributions centered on 4 and 6 μm, while the oral mode yields a distribution of larger droplets centered on 220 μm. Virus loading may differ between these modes as a virus, such as severe acute respiratory syndrome coronavirus 2 (SARS-CoV-2), has been shown to locate preferentially in the upper airways by Hou et al. (19). Strong individual variations in aerosol emissions were evidenced by Asadi et al. (16), which may lead to superspreading. As analyzed by Anand and Mayya (20), a probabilistic analysis shows that the smaller droplets are unlikely to contain viruses, with a size threshold that depends on viral load, itself depending on the severity of infection.

Several works have investigated evaporation dynamics and environmental dependence, including its coupling with settling in the works by Netz (21) and Netz and Eaton (22). However, complex respiratory fluids have been usually simplified as pure water or ideal aqueous solutions. These hypotheses are questionable since respiratory fluids, which should resemble saliva, contain significant amounts of proteins, such as mucins. Macromolecules generally dissolve nonideally in water, which can impact

Author contributions: K.R. conceptualized research; C.C., B.L., and K.R. developed methodology; T.M., O.A., and K.R. conducted investigation; O.A. developed software; T.M., O.A., B.L., and K.R. curated data; C.C., B.L, and K.R. performed validation; T.M., O.A., and K.R. prepared visualization; K.R. wrote the paper; T.M., O.A., C.C., B.L., and K.R. reviewed and edited the paper; C.C., B.L, and K.R. supervised study; C.C. and K.R. provided resources; K.R. performed project administration; and K.R. coordinated funding acquisition.

The authors declare no competing interest.

This article is a PNAS Direct Submission.

[1]To whom correspondence may be addressed. Email: kevin.roger@cnrs.fr.

This article contains supporting information online at https://www.pnas.org/lookup/suppl/doi:10.1073/pnas.2204593119/-/DCSupplemental.

Published August 5, 2022.

equilibrium composition and molecular transport within a drying droplet. Indeed, levitation experiments on millimetric saliva droplets by Lieber et al. (23) have notably shown an equilibrium size that did not significantly vary with relative humidity (RH), in contrast with ideal mixtures predictions (21). However, they also show experimentally that water evaporation from saliva and pure water proceeds at similar speeds (23), which conflicts with other predictions (24).

Water evaporation from respiratory fluids also leads to viruses experiencing a drastic change in their surrounding medium from an aqueous solution to a weakly hydrated protein and salt mixture. Both drying speeds and equilibrium conditions are expected to impact virus survival and depend on environmental conditions, such as RH and temperature. Pioneering studies by Marr and coworkers (25–27) have shown that virus survival could even vary nonmonotonically with humidities in saline media. This behavior has also been observed in saliva by Fedorenko et al. (28). However, drying proceeded over hours in these experiments rather than seconds for aerosols (29). Furthermore, the simultaneous impact of RH and temperature on both drying speeds and equilibrium conditions was not uncoupled, which precludes firm conclusions regarding virus survival in much smaller droplets and thus, at much smaller drying times.

Here, we propose an investigation encompassing these two complementary and coupled aspects of virus airborne transmission (Fig. 1) to answer the following questions. 1) Should nonideality be considered to describe respiratory droplets' equilibrium size after water evaporation? 2) Do nonvolatile solutes impact droplet evaporation times and environmental dependence? 3) What is the suspension time in the air of respiratory fluid droplets undergoing evaporation and sedimentation? 4) How does virus survival vary in a complex fluid aerosol with environmental parameters, such as RH and temperature? 5) Can we combine realistic size distribution inputs with the answers to these questions to rationalize transmission efficiency? For this purpose, we performed several quantitative experiments and numerical computations to uncouple the different elements of complexity in the global problem. We first measured saliva water uptake at equilibrium over the whole RH range, which deviates from ideal mixtures assumptions. This yielded realistic values of equilibrium sizes over the whole RH range. We then measured a concentration-dependent diffusion coefficient in drying saliva over the whole concentration range. From these quantitative measurements, we modeled water evaporation from air-suspended saliva droplets, which enables realistic predictions for the relevant size that would be difficult to characterize experimentally. We then calculated sedimentation times for drying droplets and evaluated the impact of fluid composition. Virus survival, defined as the percentage of viruses that remain infectious, was monitored for a surrogate ϕ_6 enveloped virus dispersed in saliva through a careful uncoupling of droplet drying from equilibrium storage. This knowledge was then combined and compared with measured size distributions to assess transmission efficiency.

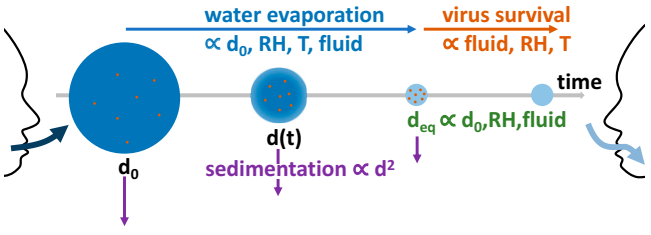

Fig. 1. Phenomena involved in airborne transmission. Droplet evaporation is a key step of airborne transmission, and it depends on initial droplet size and environmental conditions (such as temperature and RH) but also, on fluid composition. The presence of nonvolatile solutes in respiratory fluid droplets notably sets an equilibrium size and can also impact drying kinetics. Droplet sedimentation, which determines the aerosol suspension time, is thus directly impacted by the evaporation of this complex fluid. Furthermore, viruses' environment changes during drying, which can also impact their survival.

Results and Discussion

Water Content in Dried Saliva and Equilibrium Droplet Size as a Function of RH. A respiratory fluid is an aqueous solution of different nonvolatile solutes, such as proteins and salt. For instance, saliva, which composes droplets emitted in the oral mode, is composed of a variety of salts and proteins, such as mucins (30–33). Placing saliva in open air leads to water evaporation and an increase in solute concentration. If the air is dry and thus, does not contain gaseous water, the remaining mass is the nonvolatile solute mass. We measured this mass by desiccating saliva under a pure nitrogen flux, which leads to a mass fraction of 0.63% ± 0.02% for several saliva samples of different people. This value agrees with previously reported values and can be decomposed as 50% proteins (30), half of them mucins; 35% salts (31, 33); and 15% lipids (32). In practice, the air is never dry and contains a significant amount of water, which is quantified by the air RH, defined as the ratio of water partial pressure over water saturation pressure and usually displayed as a percentage. Thermodynamically, RH is thus equal to water activity in the gas. As a result, dried saliva also contains a significant amount of water, which will also directly relate to the air RH. Such a relationship between water activity and water fraction in dried saliva corresponds to the water sorption isotherm of saliva. Some works have calculated this relationship under the simplified hypothesis of thermodynamic ideality, which neglects intermolecular interactions so that mixing free energy reduces to mixing entropy (34). However, nonideality is rather expected in a complex system containing macromolecules (35), such as saliva. Deviation from ideal mixtures is quantified by measuring water content in dried saliva as a function of the air RH. The experimental sorption isotherm is displayed in Fig. 2*A* and indeed, strongly deviates from ideality displayed as an orange line. Overall, at any given humidity, there is significantly less water in dried saliva than predicted with an ideal mixture hypothesis, especially in ambient RH conditions where we observe a difference factor of two to three. Thermodynamically, this stems from intermolecular interactions and thus, mixing energy, which decreases the free energy gain upon mixing that stems from the entropic contribution. Apart from knowing precisely the water content at any RH conditions in dried saliva, which can impact virus survival as we will discuss in another section, the sorption isotherm is also a precious tool to calculate the size shrinkage of dried saliva droplets at any RH. Indeed, mass and thus, volume of both nonvolatile solutes and water are known at equilibrium at any RH, which allows us to compute the volume and thus, size ratio between initial droplets and equilibrium ones. Fig. 2*B* displays the result and compares it with the ideal mixture hypothesis (orange line). Again, significant differences are observed. Furthermore, we observe that over a large RH range from 0 to 75%, the equilibrium to initial size ratio is nearly constant around 0.2. Such a value was evidenced by direct measurements of drying saliva droplets (23, 36), which validates our approach and explains their observations. Note that this precise value can be used to correct measured size distributions of aerosols as proposed by Johnson et al. (17), where a 0.5 factor was given. Overall, RH thus does not significantly impact equilibrium droplet size over a realistic range, despite impacting water fraction.

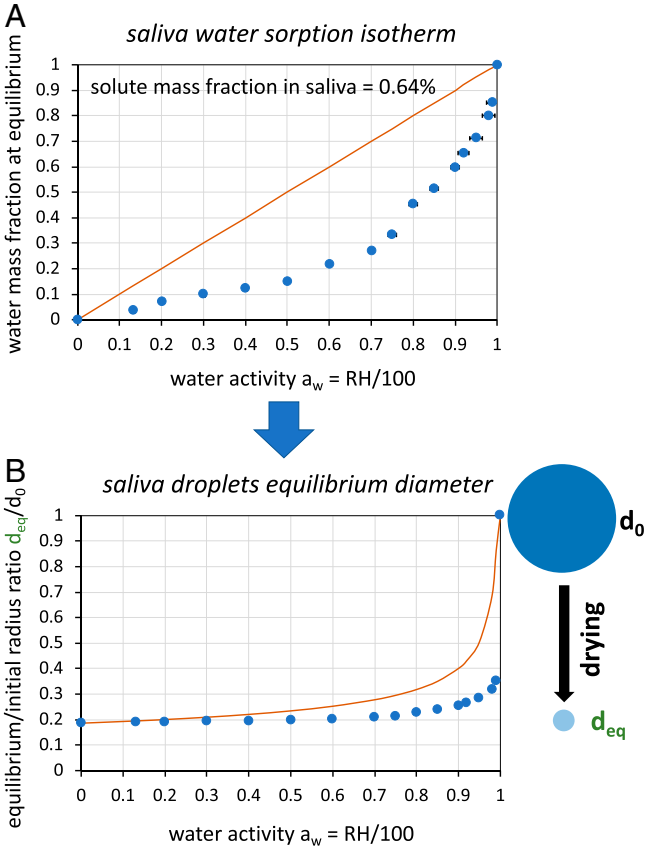

Fig. 2. Sorption isotherm and equilibrium droplet size for saliva. (*A*) Experimentally determined saliva water sorption isotherm. A strong deviation from ideal binary mixtures (red line) is observed, similar to what is observed for polymer aqueous solutions. (*B*) Calculation of the equilibrium saliva droplet diameter from the sorption isotherm. We observe that the equilibrium size is nearly independent of RH up to 75% RH and corresponds to around 20% of the initial droplet size.

Mutual Diffusion Coefficient in Drying Saliva. Water evaporation from pure water droplets is a well-described process that is controlled by water transport in the gas phase. In contrast, water evaporation from an aqueous solution of nonvolatile solutes, such as saliva, is a more complex process. Indeed, transport may become limited in the liquid phase when forming a water-poor crust at the air/liquid interface. This change in the limiting step can be predicted if one knows accurately the mutual diffusion coefficient of the aqueous mixture. Yet, previous works have rather estimated this coefficient with simplifying hypotheses, such as assuming that saliva was a saline aqueous solution (21) or by postulating a value typical of concentrated polymer solutions (24), which yield contradicting conclusions. We thus performed a direct determination of the mutual coefficient of saliva, assuming that saliva could be described as a solute/water binary mixture.

For this purpose, we first measured concentration gradients developing when evaporating water from saliva in a drying setup designed by Roger and coworkers (37–39). This setup consists of a capillary with one end placed in an airflow of controlled RH and attached on the other end to an infinite reservoir containing the aqueous dispersion, as schematized in Fig. 3*A*. Water evaporation at the air/liquid interface triggers unidirectional advection from the reservoir toward the air/liquid interface. Additionally, the water chemical potential difference between the air and the reservoir leads to a counterdiffusive flux. As a result, we obtain a concentration gradient that propagates linearly with the square root of time. Using Raman microscopy, it is thus possible to measure, throughout the gradient, the amplitude of Raman bands specific to water bonds or hydrocarbon bonds (39). This leads to an experimental measurement of concentration gradients with time that can be rescaled to a single master curve by using the mixed variable x, which is the distance z divided by the square root of time $t^{1/2}$. Typical results are displayed for several samples and times in Fig. 3*B*, showing that solute concentration decreases from the air/liquid interface toward the reservoir. This concentration gradient is a direct signature of the mutual diffusion coefficient, and we propose an original method to extract it that is fully detailed in *SI Appendix* and summarized below. The setup imposes unidirectional mass transport following an advection/diffusion equation derived from mass conservation:

$$\frac{\partial \Phi}{\partial t} = v(t)\frac{\partial \Phi}{\partial z} + \frac{\partial}{\partial z}\left(-J_{diff}\right) \qquad [1]$$

where Φ is the solute volume fraction, z is the distance from the air/liquid interface toward the reservoir, t is the time, v is the

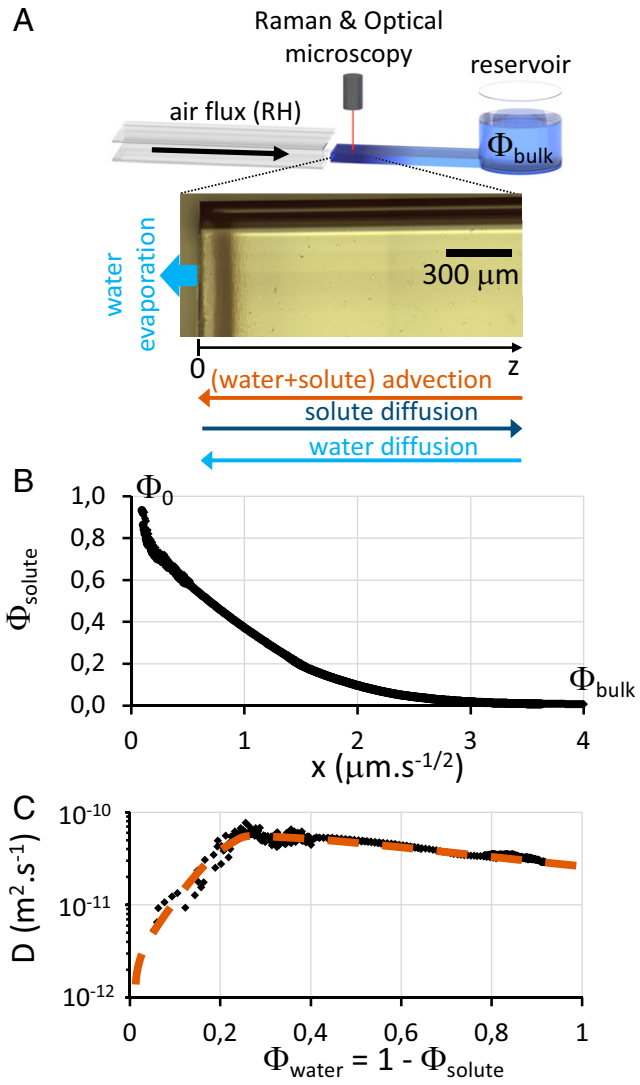

Fig. 3. Mutual diffusion coefficient in saliva. (*A*) A schematic of the unidirectional drying setup used to measure concentration gradients building up upon drying saliva at controlled RH. (*B*) Typical concentration profiles obtained at RH = 0% at two different times, rescaled by the space/time variable x = distance/time$^{(1/2)}$. (*C*) Fickian mutual diffusion coefficients obtained numerically from the two above concentration profiles. The orange line represents the best fit of these datasets, which is used in the following for calculations.

advective flow, and J_{diff} is the diffusion flux. Fick's law expresses this diffusion flux as:

$$J_{diff} = -D_{Fick}(\Phi)\frac{\partial \Phi}{\partial z} \quad [2]$$

where D_{Fick} is the Fickian mutual diffusion coefficient. Our setup also conveniently sets two constant boundary conditions. At the air/liquid interface ($z = 0$), the net solute flux is zero since solute is nonvolatile; toward the reservoir [$z \to \infty$ and $\Phi(z, t) \to \Phi_{bulk}$], the diffusion flux goes to zero. Together with a change of variable to $x = z/t^{1/2}$, Eq. **1** can be rewritten as:

$$J_{diff}(x) = \frac{1}{2}\int_0^x \tilde{x}\frac{d\Phi}{d\tilde{x}}d\tilde{x} - \frac{\Phi(x)}{2\Phi_{bulk}}\int_0^\infty \tilde{x}\frac{d\Phi}{d\tilde{x}}d\tilde{x} \quad [3]$$

with the following direct link to the diffusion coefficient:

$$D_{Fick} = \frac{-J_{diff}}{d\Phi/dx} \quad [4]$$

From the experimental data of Fig. 3*B*, $\Phi(x)$, we can calculate $D_{Fick}(x)$ and thus, $D_{Fick}(\Phi)$. The result of this analytical inversion procedure is displayed in Fig. 3*C*. We observe a strong collapse of the diffusion coefficient with increasing volume fraction above 70% in solute, which evidences that water transport is hindered in concentration gradients building up at the air/liquid interface.

Drying of Suspended Respiratory Fluids. The experimental monitoring of water evaporation from suspended droplets is challenging and is often addressed by using either levitation setups or superhydrophobic ones. However, monitoring is limited to droplets typically large enough to be imaged with a camera. Furthermore, controlling the airflow in such setups is challenging. Therefore, we propose a strategy in which water evaporation is calculated using robust models and parameters and compared against experimental values obtained by drying (large) droplets deposed on a superhydrophobic substrate with a controlled airflow. Simple models exist for modeling water evaporation from pure water droplets, and the simplest assumes that water transport is limited in gas and purely diffusional (21). Improvements typically include convective effects as a correction through the use of a Sherwood number, Sh, leading to:

$$\rho_l\frac{dR}{dt} = -\frac{ShD_g\rho_v}{2R(t)}(Y_g - Y_{g,\infty}(RH)) + \rho_l\frac{dR}{dt}Y_g \quad [5]$$

with ρ_l being the droplet density, D_g being the water diffusion coefficient in air, ρ_v being the vapor density, Y_g being the water mass fraction in the air at the drop vicinity, and $Y_{g,\infty}(RH)$ being the water mass fraction in the air far from the drop (*SI Appendix*, Fig. S1). Typically, the convective effects are considered through the correlation of Frossling (40), which gives the Sherwood number as a function of flow properties (*SI Appendix*). Other effects, such as the influence of the evaporating mass flow on the velocity field around the droplet, can also be considered through the use of a modified Sherwood number (41).

In principle, thermal effects should also be considered since water evaporation is an endothermic process. Indeed, using a purely diffusional model, Netz (21) calculated an evaporation-induced temperature drop equal to 10 °C at RH = 50%, independently of the droplet size. Yet, we have rather performed an isothermal computation without including such effects as they are mostly compensated for by other factors. For instance, droplets are actually expelled from the air tract at a higher temperature than ambient conditions and contain nonvolatile solutes, which were shown by Rezaei and Netz (35) to decrease the temperature drop magnitude. Also, experimental drying times measured at RH = 0 (Fig. 4*B*) and 60% are adequately fitted by our modeling using a realistic value of the airflow velocity. Finally, the overall correction would account for the uncertainty of a few micrometers in initial droplet size, which is in line with other possible corrections, such as the local RH in an aerosol compared with its surroundings (4).

Furthermore, a different modeling approach is anyway required when water transport becomes limited in the droplet rather than in the gas. This transition arises in aqueous solutions when nonvolatile solutes sufficiently accumulate to drastically decrease mutual diffusion (39, 42), as observed for instance in the previous unidirectional experiment. This transition is controlled mainly by droplet size, transport in air, solute concentration, and the variation of the mutual diffusion coefficient in the aqueous solution. The latter was precisely determined in the previous section and can thus be used quantitatively to predict the effect of solute gradients on transport, in contrast with ad hoc estimates that may largely differ (24, 35). Since transport may be limited in either gas or liquid phases depending on the drying stage, they must be both taken into account in a full model. This requires solving a one-dimensional diffusional transport equation in the spherical coordinate system $0 \le r \le R(t)$:

$$\frac{\partial \Phi}{\partial t} = \frac{1}{r^2}\frac{\partial}{\partial r}\left(r^2 D_{Fick}(\Phi)\frac{d\Phi}{dr}\right) \quad [6]$$

The solving can be done by writing the continuity of water flux at the air/liquid interface and two boundary conditions stating that the net solute flux is zero at the air/liquid interface and ensuring symmetry at the center of the drying droplet (*SI Appendix* has a detailed derivation). A numerical procedure using a variable transformation (42) then yields $R(t)$, whether transport is limited in the gas or the liquid phase, with the realistic D_{Fick} as input. We verified that this procedure yielded the analytical prediction for pure water when the solute concentration tends toward zero, as displayed in *SI Appendix*, Fig. S2.

The outcome of such simulations was first compared against experimental data of sessile droplets on a superhydrophobic substrate placed in a homemade drying cell of controlled airflow and RH, schemed in Fig. 4*A*. Experimental and numerical results are displayed for both water and saliva droplets at RH = 0% in Fig. 4*B* and show that solute effects remain modest. Furthermore, the good agreement between experiments and simulations data demonstrates that our simulations can be used to assess quantitatively saliva droplet evaporation. For instance, Fig. 4*C* compares the evaporation of 80 μm water or saliva droplets at different RHs. We see that evaporation proceeds overall similarly to pure water, except at the end of the drying process when diffusion in the liquid becomes limiting. *SI Appendix*, Fig. S3 displays typical concentration gradients that develop upon drying such droplets. An evaporation time can be extracted from these curves and compared with the reference case of pure water, as displayed in Fig. 4*D*. As RH decreases or droplet size increases, the deviation due to solutes increases but remains quite modest due to low initial solute concentration. However, our model also allows us to modify solute concentration above that of saliva that may be relevant to respiratory fluids. This increases the effect of gradients and slows down evaporation. However, these effects only develop toward the end of the drying process for realistic solute concentrations. Overall, solute effects are not significant in the evaporation of

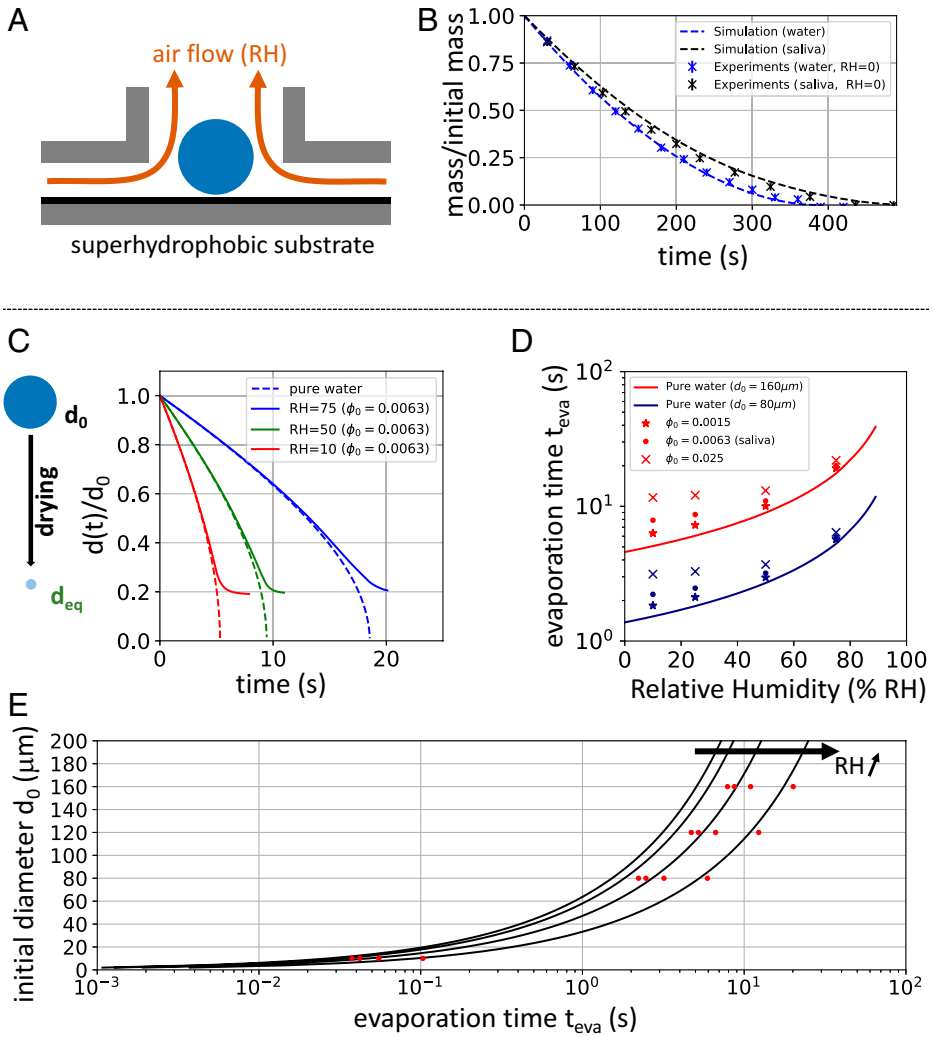

Fig. 4. Evaporation of saliva droplets. (*A*) Scheme of a droplet drying setup, where a liquid droplet is deposited on a superhydrophobic Teflon-thiolated nanosilver coating and surrounded by an airflow of controlled RH. (*B*) Ten-milligram droplet drying kinetics for both water and saliva at RH = 0% and numerical calculations using the experimentally determined diffusion coefficient obtained in Fig. 3. The agreement supports the validity of our modeling. (*C*) Modeled droplet evaporation for water and saliva droplets at different RHs, showing that solutes impact evaporation times only at the end of the process. (*D*) Evaporation times for water, saliva, and saliva-like fluids at either lower or higher solute concentration for two droplet sizes. Evaporation is increasingly slowed down upon increasing solute concentration, which can be the case in the lower respiratory tract. Still, the effect is mostly observed at the end of the drying process. (*E*) Evaporation time for water droplets (black lines) and saliva (red dots) at increasing RHs (10, 25, 50, 75%).

respiratory fluid droplets, as illustrated over a realistic size range in Fig. 4*E*, since solute concentration is low, droplets are small, and our results can quantitatively settle this issue thanks to realistic inputs. Note that the development of gradients and the slowing of evaporation toward the end of the drying process are negligible when evaluating the aerosol sedimentation time as we will see in the following section. Still, gradients impact viruses' environment during drying, which may, in turn, impact virus survival as we will discuss later.

Drying and Sedimentation Competition of Respiratory Droplets. One important factor for airborne transmission is how long droplets remain suspended in air before falling to the ground. Gravity is the driving force to settling, and the corresponding sedimentation time, for these small droplets in the Stokes regime, is inversely proportional to the square of droplet radius:

$$t_{sedi} = h.\frac{9.\mu_g}{2g\rho_l R_0^2}, \qquad [7]$$

where h is the height at which the droplet is emitted (set to 1.5 m), μ_g is the viscosity of air, ρ_l is the density of the droplet, g is the gravitational acceleration, and R_0 is the radius of the drop.

In an aerosol, evaporation takes place until an equilibrium droplet size is reached, which significantly modifies sedimentation times. Two limiting cases for estimating the settling time can be described. 1) When droplets are large enough that they settle much faster than they evaporate, evaporation can thus be neglected in assessing the settling time. 2) When droplets are small enough that they dry before they settle, the sedimentation time is thus calculated with the equilibrium droplet mass after evaporation as given by the sorption isotherm. Two sets of curves giving the sedimentation time for both limiting cases can thus be obtained. Since the sorption isotherm is rather flat up to high RH, the equilibrium mass does not significantly vary with RH. However, it is much lower in absolute value than what could be estimated with ideal mixtures hypotheses. The experimental value is thus crucial to obtaining realistic figures. The transition from one set of curves to another can be calculated since we know both drying kinetics and the sedimentation law, and it is displayed in Fig. 5. The transition depends on the value of RH and is rather sharp. The resulting settling times thus increase abruptly by an order of magnitude when reaching this threshold. Indeed, water evaporation leads to a decrease by 5 of the radius and thus, by 25 of the settling time.

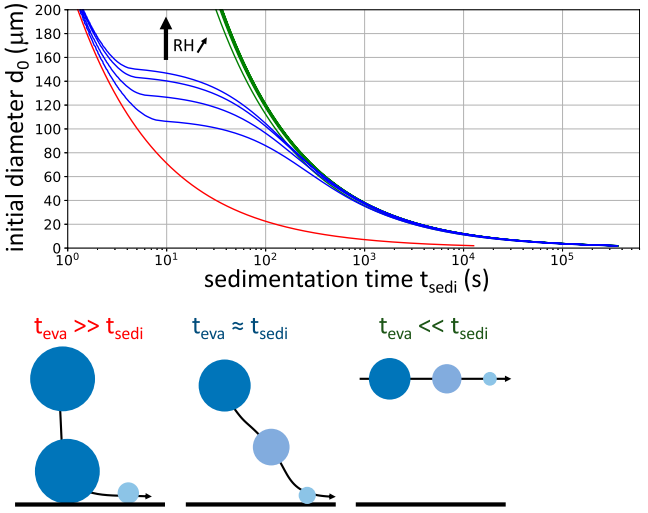

Fig. 5. Sedimentation times of evaporating droplets. Sedimentation times for droplets that do not evaporate (red line), instantly evaporate (green lines), or evaporate as they fall (blue lines) as a function of RH (10, 25, 50, 75%). An intermediate region is observed where sedimentation times increase by an order of magnitude, and its position depends on RH and temperature (*SI Appendix*, Figs. S4 and S5).

Virus Survival in Drying Droplets at Different RH and *T*: Uncoupling the Kinetic Stage from the Equilibrium One. We now turn to assess the role of respiratory fluid with respect to virus survival when drying virus-loaded droplets. Here, survival or viability should be understood as the possibility for a virus to remain infectious, which may be compromised by denaturing either its spike proteins or its RNA/DNA. Pioneering studies by Marr and coworkers (1, 25–27) have evidenced nonmonotonic RH dependence of SARS-CoV-2 and ϕ6 viruses. However, viruses were dispersed in buffer media rather than a physiological fluid. Yet, the water activity/composition isotherm of saliva evidences the preponderance of polymeric solutes, proteins, rather than salts in the physicochemical behavior of saliva. Survival experiments in saliva are thus required to obtain robust conclusions. Fedorenko et al. (28) performed such a study on three different viruses dispersed in human saliva and observed similar trends as Marr and coworkers (1, 25–27). However, in all these studies, drying is typically taking place within hours, which strongly deviates from the timescales involved when drying aerosols obtained in the previous section. Furthermore, Fedorenko et al. (28) have only evaluated survival after 14 h, which precludes a kinetic analysis. Finally, it seems necessary to distinguish two stages for virus survival (Fig. 6*A*): the drying stage where water evaporates and the suspended stage where thermodynamic equilibrium is reached following the activity/concentration relationship. Since RH impacts both stages, we thus proceeded to two types of experiments to uncouple and quantify the impact of both stages on virus survival.

We first evaluated viability at the end of the drying stage for two droplet sizes (2 and 4 mm) (Fig. 6*B*), which correspond to different evaporation times and gradient extent. We observed a 10-times-larger viability for the smaller droplets than for the larger ones, which suggests that viruses experience drastically different conditions in small and larger droplets. As shown by our calculations, protein gradients are more pronounced for larger droplets, and after drying, proteins are mainly deposited as a dense layer at the rim. Concomitantly, we observed that in large droplets, salts were crystallized at the center of the droplet. Viruses are colloidal particles, and they are expected to diffuse away from the protein-rich layer and thus, face larger salt concentrations in the

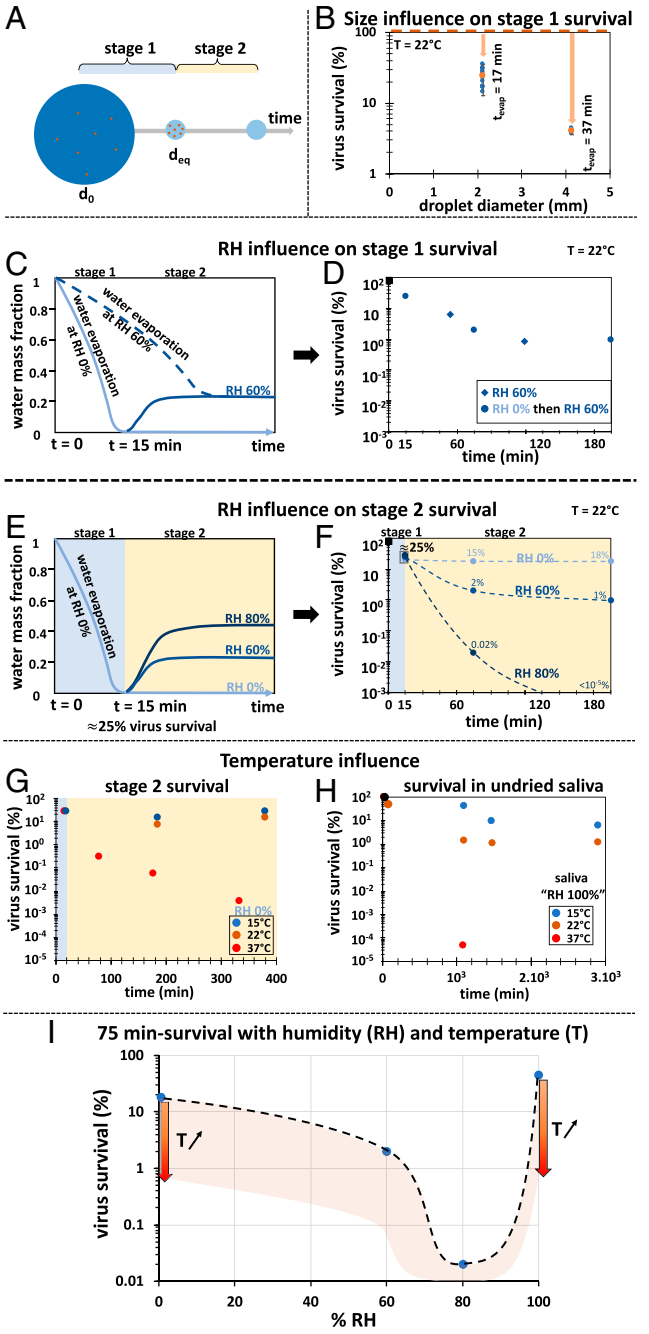

Fig. 6. Virus survival with RH and temperature (T) in drying aerosols. (*A*) Two different stages should be considered to evaluate virus survival; the first stage involves water evaporation, while the second stage corresponds to equilibrated droplets that remain suspended in the air. (*B*) ϕ6 survival (percentage of viruses that remain infectious) in dried saliva droplets at RH = 0% at t = 17 and 37 min, which correspond to drying times for droplet diameters of 2.12 and 4.13 mm, respectively. The two orange points represent the means of each data series, with the error bars representing the typical SDs. (*C*) Drying pathways corresponding to a different stage 1, drying at RH = 0%, and then, equilibration to 60% or direct drying at RH = 60% but the same stage 2. (*D*) Corresponding virus viability, which shows that the two pathways yield similar results. (*E*) A general description of the protocol composed of two stages. Stage 1 corresponds to the water evaporation from 5-µL saliva droplets at RH = 0%. In stage 2, once the thermodynamic equilibrium is reached upon evaporation (t = 15 min), the dried droplets are equilibrated at different RHs (0, 60, and 80%). (*F*) Virus viability was determined as a function of time and RH in stage 2. (*G*) ϕ6 viability in dried saliva droplets of 5 µL at RH = 0% as a function of time at three different temperatures: 1 °C, 22 °C, and 37 °C. (*H*) ϕ6 viability in liquid saliva as a function of time and at three different temperatures: 15 °C, 22 °C, and 37 °C. (*I*) Summary figure from panels *E*–*H* displaying virus survival after 75 min at T = 22 °C. A nonmonotonic RH dependence of virus survival is observed, while survival also overall decreases with increasing temperature.

center of the drying drop, which is detrimental to their survival. Here, we must stress that droplet sizes are far too large compared with what is relevant for airborne transmission. However, this experiment can be used to extrapolate that reducing droplet size should lead to an enhanced survival at the end of stage 1 and thus, that stage 1 is not limiting for virus survival. As a confirmation, we performed two drying experiments that differ only in stage 1 but display the same stage 2. We either dried the droplet at RH = 0% before equilibrating it at RH = 60% or dried the droplet at a constant RH = 60% (Fig. 6*C*). We observe in Fig. 6*D* that both experiments yield similar outcomes within experimental error, which confirms that the RH at which droplets are dried during stage 1 and thus, drying kinetics are not crucial when droplets are small enough. Note that dispersing viruses in either buffer or pure water yielded similar survival rates at the end of stage 1, so we did not observe any medium effect in this stage.

We then turned to an evaluation of the second stage in which droplets have reached their equilibrium size. To uncouple it from stage 1, we fully dried several droplets at the same RH of 0% and then, displaced their equilibrium by changing systematically RH and monitoring viability over time. We can thus compare droplets that experienced the exact same drying stage 1 but are placed in different storage conditions (stage 2), as shown in Fig. 6*E*. We first observe that keeping RH to 0% leads to constant virus viability, which contrasts with the survival collapse observed by Fedorenko et al. (28) at 14 h when dispersing viruses in pure water. This suggests that water-deprived saliva is an excellent means to keep enveloped viruses intact on surfaces for an extended period of time and that the medium matters for stage 2 survival. Such fomites remain infectious for at least several hours. Note that this protective effect of saliva contrasts with a recent study suggesting that mucins rather decrease virus infectivity through interactions with their spike proteins. Yet, such effects were observed at 10-times-larger mucin concentrations than saliva's content. Also, the used bovine mucin is actually only partially soluble in water in contrast with saliva, as also noted by Verejano and Marr (25), which suggests additional effects upon drying, such as virus encasing in a hydrophobic medium. Finally, such an observation would mean that any transmission route, fomite or airborne, would be severely hindered by mucins, which are natively present in respiratory fluids, and would thus conflict with the high observed transmissibility of coronaviruses.

Since stage 2 is shown to control virus survival in drying droplets, it is informative to display virus survival at this stage as a function of RH, shown in Fig. 6*F*. The resulting curve displayed in Fig. 6*I* displays a nonmonotonic variation of the virus survival, at 75 min after droplet generation, as a function of RH. Such a "U shape" was also observed by Morris et al. (26) for several enveloped viruses in buffer media but involved experiments in which drying stages 1 and 2 remain coupled and salt was the major nonvolatile solute at play. In our study, we evidenced that in saliva, proteins are predominant over salts in the overall behavior, which discards salt efflorescence as the key quantity to explain the presence of a minimum. While this fascinating observation clearly deserves further investigation, our work actually provides mechanistic insights to explain this nonmonotonic variation. First, it is important to recall that any nonmonotonic variation must result from at least two competing contributions. As water content decreases, water activity also decrease, which can be translated as an osmotic pressure increase. Together with other possible solute effects upon decreasing water content, such as pH variations or increasing enzymes concentration, this osmotic contribution should decrease virus survival upon decreasing RH. Yet, another contribution emerges from our molecular transport data. Indeed, we observe in Fig. 3*C* that molecular transport collapses when $\phi_{water} < 0.25$, which corresponds to RH = 70% according to Fig. 2*A*. This behavior typically corresponds to a glass transition from a liquid-like state to a solid-like one. Thus, decreasing RH below this transition leads to encasing viruses in arrested surroundings, which efficiently protects them from degradation. Interestingly, a similar explanation was recently put forward by Huynh et al. (43), who observed rheological changes with RH when colliding droplets containing different model suspension media.

We also investigated the impact of temperature on survival both for dried droplets at RH = 0% (Fig. 6*G*) and in liquid saliva (Fig. 6*H*). In dried saliva, virus survival is similar at 1 °C and 22 °C but decreases at 37 °C. In liquid saliva, no decay was observed at 1 °C, but survival was otherwise observed to decay with increasing temperature. We can thus conclude that increasing temperature is detrimental to virus survival at all RH.

Overall, these experiments evidence the environmental impact of both RH and temperature on virus survival. Survival within dozens of minutes decreases when increasing RH or increasing temperature, but effects at shorter times will remain modest.

Assessing Transmission Efficiency. Throughout this manuscript, we have quantified the role of the respiratory fluid on both droplet evaporation and virus viability and its environmental dependence notably with RH. This knowledge can now be used to assess transmission efficiency, which requires a quantitative input regarding emitted droplet size. While this important parameter is sometimes discussed using only average numbers, a realistic discussion must actually take into account the entire size distribution. Several experimental works have provided such characterizations, although often partial ones due to the use of a single sizing technique. As shown notably by Johnson et al. (17), two populations of droplets are measured when using two different techniques, which dispels any apparent contradictions of the literature (15–18). Johnson et al. (17) identified two main populations: 1) a population of droplets from 0 to 38 μm that actually corresponds to two subpopulations, with the smallest being produced in the bronchioles (breathing aerosol) and the larger one produced in the larynx (vocalization aerosol), and 2) a population of droplets from 38 to 1,000 μm that is produced in the oral cavity between the lips and epiglottis. Many studies have focused on the first population because it represents the majority of droplets produced. Yet, it represents only a very small fraction of the total volume emitted as pointed out by Lieber et al. (23). This difference between number and volume distribution is quite important for the discussion, as the volume distribution is much more relevant to discussing viral load and thus, transmission. Volume distributions, calculated from measurements by Johnson et al. (17), when speaking or coughing are thus both displayed in Fig. 7*A*, taking into account a corrected evaporation factor obtained from our experimentally determined sorption isotherm. Both distributions are similar, evidencing the robustness of the description. We also plotted isotime curves corresponding to a given sedimentation time as a function of RH in Fig. 7*B*, as obtained from Fig. 5. This firstly shows that a cutoff around 100 μm is realistic since larger droplets fall too quickly to contribute to airborne transmission. We can thus define two types of aerosol: an aerosol composed of droplets that remain suspended for hours and an aerosol composed of droplets that remain suspended for minutes.

The hours aerosol is produced in the bronchioles and the larynx, and it represents 77% in number but only 0.009% in volume. Most of this volume actually corresponds to droplets

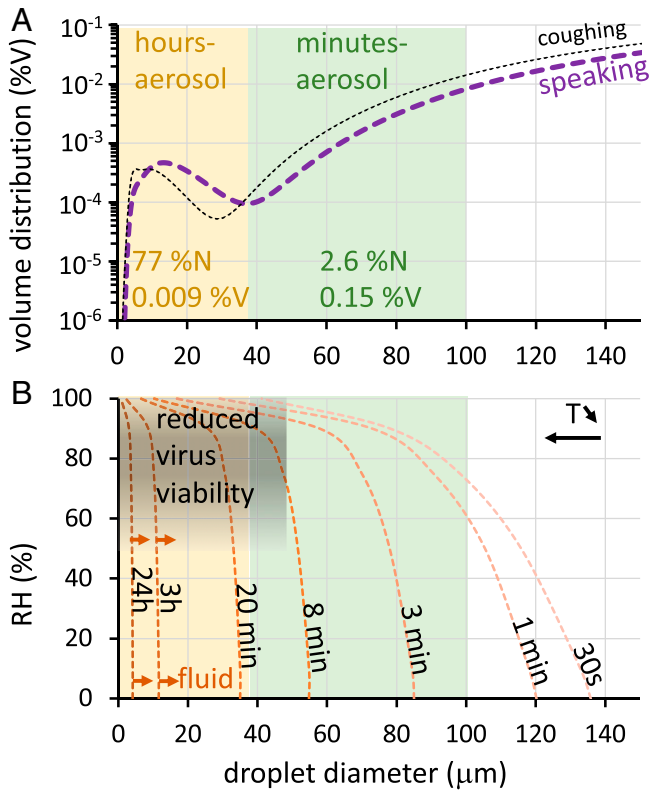

Fig. 7. Two distinct aerosols matter for airborne transmission. (*A*) Volume size distributions recalculated from Johnson et al. (17) using data from Fig. 2 for aerosols emitted through speaking or coughing. (*B*) Isosedimentation times curves obtained from Fig. 5. Two distinct aerosol populations can be identified: a population of numerous droplets (77% in number) but of a very small overall volume, emitted mainly in the larynx, that can remain suspended for hours (hence, termed hours aerosol) and a population representing a much larger volume emitted in the oral cavity that can remain suspended for minutes (hence, termed minutes aerosol). The gray area recalls that virus viability at longer times is compromised upon increasing RH, as shown in Fig. 6. Note that RH decreases aerosol suspension time, notably for the minutes aerosol over the whole RH range, while the hours aerosol is only impacted at very high RH consistently with the sorption isotherm displayed in Fig. 2.

produced in the larynx, and droplets produced through breathing are thus even more negligible. The fluid composition of these droplets may deviate from saliva with enhanced phospholipid concentration and possibly protein concentration. This will delay evaporation and can actually decrease aerosol lifetime if solute concentration becomes large enough, although the overall effect should remain modest as calculated from Fig. 4. We have also identified in Fig. 6 that virus viability could be drastically reduced at longer times upon increasing RH, which primarily impacts this population, as displayed in Fig. 7*B*. RH also impacts suspension time but only at very high humidities, consistently with the sorption isotherm and evaporation being very fast for such small droplets. This population accumulates in the air and can be traced using air quality measurements. This storing capacity increases the effective viral load, although such an effect can be effectively countered by frequent air renewal.

The minutes aerosol is produced in the oral cavity, and it represents only 2.6% in number but 0.15% in volume, which is considerably more than its laryngeal counterpart. Droplet composition has been shown to be close to saliva (17). Since its lifetime is much shorter, virus viability is not expected to be a major contribution. Increasing RH over the whole RH range is, however, much more impactful than for the other population as evaporation times are more similar to sedimentation times, which correspond to the wave displayed in Fig. 5. This population does not accumulate in the air of an enclosed environment and thus, cannot be traced very efficiently from air quality measurements. Yet, its much more significant volume fraction means it may carry a much higher viral load (20). Continuous air renewal and social distancing are required to hinder transmission from minutes aerosol, while frequent but discontinuous air renewal will not have much impact if the time interval is larger than the typical suspension time of a few minutes.

Overall, this discussion shows two protagonists for airborne transmission and highlights that minutes aerosols are likely more prominent than hours aerosols, which received most of the attention in recent literature. Interestingly, an increase in RH is an effective means to reduce transmission efficiency for both types of aerosols and should be considered as a mitigation tool. Temperature is in contrast a double-edged variable since decreasing temperature decreases suspension time but increases virus viability. Decreasing temperature is thus detrimental to the transmission by minutes aerosol but rather favorable for hours aerosol.

Conclusion

The purpose of this work was to evaluate quantitatively the role of fluid complexity in the airborne transmission of viruses and its interplay with environmental variables (such as RH and temperature) and provide guidelines for assessing transmission efficiency. Our approach was thus to investigate simultaneously all the different stages involved after the emission of a dispersion of droplets, or aerosol, as depicted in Fig. 1. Like any polymer solution, saliva displays a nonideal mixture behavior, which results in a weaker increase of water fraction with the air RH over most of the humidity range (Fig. 2*A*). Consequently, droplets dry to equilibrium sizes that are both smaller and less dependent on RH than predicted with ideal mixtures models (Fig. 2*B*). This notably slows down their sedimentation and increases aerosol suspension time. While nonvolatile solutes are also expected to slow down water evaporation due to gradients buildup and thus, a decrease in water transport (Fig. 3), we have shown this effect to be negligible for saliva due to its low solute concentration of 0.64% (Fig. 4). Still, our model also allows for calculating the impact of increasing solute concentration, which might be relevant when the respiratory fluid is more concentrated than saliva, notably for the smallest droplets emitted in the bronchioles or the larynx. Therefore, evaporation might be significantly delayed (Fig. 4), which is rather suggested to decrease virus viability due to gradients formation (Fig. 6*B*). We have also shown that enveloped viruses remain viable for hours in water-deprived saliva (Fig. 6*F*). Encasing viruses in a water-deprived polymeric network thus appears like an interesting strategy to preserve viruses. This preserving effect is progressively lost upon increasing RH and thus, water amount (Fig. 6*F*).

Comparison of this knowledge with the size distribution of emitted droplets evidences two distinct aerosols (Fig. 7): a population of 0- to 40-μm droplets that can remain airborne for hours or "hours aerosol" and a population of 40- to 100-μm droplets that remains airborne for minutes or "minutes aerosol." Apart from their suspension times, these two aerosols have other distinct features that are crucial to assessing their transmission potential. The hours aerosol is mostly emitted in the larynx and in a smaller part in the bronchioles. It is likely composed of droplets enriched in lipids and proteins compared with the minutes aerosol emitted in the oral cavity that has a composition close to saliva. This can slightly decrease the suspension time of the hours aerosol compared with predictions, consistently with Fig. 4. Furthermore, while the hours aerosol corresponds to the majority of droplets

in number, which explains why it has been under intense recent scrutiny, it represents a much lower volume than the minutes aerosol. Consequently, the viral load of the minutes aerosol should be much larger than that of the hours aerosol, an assumption that must be tempered with the spatial variation of the viral load along the airways. Still, in the case of COVID-19, the viral load has been shown to be higher in the upper airways than the lower ones (19) and even more so for more contagious variants such as, variant omicron (44). Therefore, while the competition in transmission efficiency is disease dependent, its assessment is shown to result from the simultaneous combination of the viral load distribution along the respiratory tract and the size distribution of emitted droplets. At least for COVID-19, we can thus conclude that minutes aerosols, rather than hours aerosols, dominate the transmission efficiency.

Turning to environmental factors, both aerosols remain suspended longer when decreasing RH (i.e., in dried air) as evaporation is enhanced. However, this impact is much more pronounced on the minutes aerosol. Increasing RH also decreases virus viability for any droplet size, but this effect will develop over longer times than a few minutes and will rather impact the hours aerosol, decreasing virus survival at longer times. Increasing the air humidity is thus an unambiguous means to decrease transmission. In contrast, temperature has two opposite effects as higher temperatures increase suspension times but decrease virus viability. Since an hours aerosol corresponds to evaporation times much faster than sedimentation times (Fig. 5), the long-term effect of temperature on survival will predominate. Increasing temperature thus decreases transmission by minutes aerosols. In contrast, transmission by minutes aerosol is rather controlled by their suspension time, and thus, increasing evaporation time by decreasing temperature is more important than survival effects that are not significant within 10 min.

Overall, humid and cold air is thus preferable to decrease transmission. Note that while this may seem contradictory with winter-enhanced propagation of airborne viruses, it is worth recalling that while the outside air tends to be colder and more humid in winter, the inside air tends, in contrast, to be drier due to heating.

Finally, we would like to stress that both aerosols have different suspension times and thus, ability to accumulate in a closed environment. The ability of hours aerosol to accumulate, thus increasing its effective viral load in the air, is easily remediated by regular aeration, and accumulation could be tracked through air quality measurements, such as CO_2 concentration. In contrast, removing minutes aerosols would require constant aeration to renew the air or social measures, such as distancing and wearing masks, which efficiently filter micrometric or larger droplets (45). Interestingly, the contribution of breathing to the minutes aerosol is negligible, and even within the hours aerosol, it represents a much lower volume than laryngeal emission. Therefore, breathing with a closed mouth should not contribute significantly to propagation but of course, does not protect against contamination itself.

This work shows that bringing together different fields is necessary to address a transdisciplinary problem, such as airborne transmission, and provides knowledge useful to address both COVID-19 transmission and more generally, airborne transmission. Furthermore, we show that building a quantitative tool to assess virus transmission requires a solid description of transport processes taking place in and around drying droplets together with a virus-specific experimental characterization of three main factors that should be the focus of future investigations: the viral load distribution in the respiratory system, the fluid composition of emitted droplets in the lower air tract, and virus survival in physiological dried fluids.

SI Appendix. *SI Appendix* provides detailed mathematical derivations and displays typical concentration gradients, evaporation, and sedimentation times at different temperatures.

Materials and Methods

Materials. Sodium Magnesium (SM) buffer was prepared by mixing NaCl, $MgSO_4$, *tris*(hydroxymethyl)aminomethane · HCl, and gelatin in water. NaCl > 99.5%, $MgSO_4$ Bio Reagent, Trizma hydrochloride > 99%, silver nitrate 99.9999%, tryptic soy agar (TSA), tryptic soy broth (TSB), agar, and 3,3,4,4,5,5,6,6,7,7,8,8,9,9,10,10,10-heptadecafluoro-1-decanethiol were bought from Sigma Aldrich. Bacteriophage $\phi 6$ and the host bacteria *Pseudomonas syringae* were purchased from DSMZ. Saliva was provided by two volunteers and collected by unstimulated drooling in a sterile centrifugation tube for a few minutes prior to each experiment.

Sorption Isotherm: Activity/Composition Relationship. Human saliva (5 g) was dried out at RH = 0%, which yielded the solute fraction of saliva (0.64%). Then, the sample was progressively rehydrated by increasing RH stepwise. We measured the mass uptake after equilibration at each step (>2 h). The absence of hysteresis was checked, and the experiment was repeated three times.

Unidirectional Drying Cell and RH Control. The drying cell was made of a rectangular borosilicate capillary with a cross-section of 0.1 × 1 mm^2 and a length of a few centimeters, and the setup was fully described in previous publications (37–39, 42). One end of the capillary was connected to a small capped plastic cylinder, which served as a reservoir. The other end, which was cleanly cut, was opened and placed under an airflow of controlled RH, generated by a HumiSys instrument from InstruQuest Inc.

Raman Confocal Microscopy. Raman experiments were performed on a WITec alpha 300R confocal Raman microscope with a 532-nm laser wavelength (power 54 mW). Each spectrum is the average of 20 measurements of 14.5 ms (detector in the electron multiplying charge-coupled device mode). On a given line, spectra were acquired every micrometer, with a 50-times long-distance objective (numerical aperture: 0.55, working distance: 8.7 mm; ZEISS EPI "Achromat ELWD"), which gives a lateral resolution of around 500 nm and a depth resolution of around 2.8 μm. We verified the absence of sample damage over time due to laser exposure. Composition gradients were obtained from the resulting spectra series using a two-component fitting procedure based on the spectra of pure water and fully dried saliva.

Preparation of a Superhydrophobic Surface and Drying Kinetics of Sessile Droplets. A superhydrophobic coating was synthesized on copper adapting the protocol from Larmour et al. (46). After sanding and surface reduction with ascorbic acid, the copper piece was immersed in a 10 mM silver nitrate solution for a few minutes. Silver ions were spontaneously reduced into silver atoms by copper surface atoms (galvanic corrosion), and the resulting surface was then rinsed with water and dried. A fluorothiol solution in dichloromethane was then deposited on the surface, left to evaporate, rinsed with dichloromethane, and dried. A liquid droplet (water or saliva) was deposited on this superhydrophobic surface, which was placed in a homemade air chamber. Air flowed all around the deposited droplet, ensuring symmetry. Droplet weight was measured over time.

Drying of Virus-Loaded Droplets. Five-microliter droplets containing viruses were deposited on a plastic surface and dried with an airflow of controlled RH.

Microbiology. Experiments were performed under sterile conditions. *P. syringae* bacteria (from DSMZ German Collection), were suspended in TSB at room temperature in the dark and under agitation. After about 48 h, the sample was turbid, and the optical density (OD) measured with ultraviolet-visible spectroscopy at 600 nm (OD 600) was equal to 0.3. The propagation of $\phi 6$ viruses was performed by the bacterial host addition, as recommended by the Leibniz Institut DSMZ. Viruses were suspended in a bacterial suspension (OD 600 = 0.3) and kept overnight at 22 °C under agitation. Then, the viral suspension was filtered (Minisart syringe filter 0.1 μm saturated beforehand with a sterile beef extract [1%] to reduce the adsorption of viruses onto the filters) to obtain a bacteria-free viral suspension. Following this amplification step, viruses

were titrated by depositing them on TSA/soft agar plates on which was grown a bacterial host culture. Such plates were prepared by first melting soft agar and then mixing it with a bacterial host culture (500 μL of bacterial suspension for 3.2 mL soft agar). It was then poured on the TSA plates to obtain the top layer on which viruses were then deposited. Each plate was partitioned into eight areas, each receiving 10 μL of the viral suspension at different dilution factors. Plates were then sealed and incubated at 22 °C for 24 h. The concentration of infectious viruses (plaque-forming unit [PFU] per milliliter) was then measured by counting the bacteria-depleted spots or plaques in the first adequate area where spots were numerous but unmerged. The typical initial $\phi 6$ concentration was within 10^9 to 10^{11} PFU/mL, a high value corresponding to highly infected hosts (20). Similar results were obtained when repeating experiments at different initial concentrations.

Data Availability. All study data are included in the article and/or *SI Appendix*.

ACKNOWLEDGMENTS. Micheline Abbas and Yannick Hallez are acknowledged for stimulating discussions and reviewing this paper, and Frédéric Da Costa, Vincent Loisel, and Jean-Pierre Escafit are acknowledged for the manufacturing of the droplet evaporation setup. Agence Nationale de la Recherche is acknowledged for financial support through Grants ANR-17-CE- 09-0004-01 COATING and ANR Eva-COVID.

Author affiliations: [a]Laboratoire de Génie Chimique, Université de Toulouse, CNRS, Institut National Polytechnique de Toulouse, Université Paul Sabatier, 31400 Toulouse, France

1. C. C. Wang *et al.*, Airborne transmission of respiratory viruses. *Science* **373**, eabd9149 (2021).
2. R. Zhang, Y. Li, A. L. Zhang, Y. Wang, M. J. Molina, Identifying airborne transmission as the dominant route for the spread of COVID-19. *Proc. Natl. Acad. Sci. U.S.A.* **117**, 14857–14863 (2020).
3. W. C. K. Poon *et al.*, Soft matter science and the COVID-19 pandemic. *Soft Matter* **16**, 8310–8324 (2020).
4. K. L. Chong *et al.*, Extended lifetime of respiratory droplets in a turbulent vapor puff and its implications on airborne disease transmission. *Phys. Rev. Lett.* **126**, 034502 (2021).
5. J. Wang *et al.*, Short-range exposure to airborne virus transmission and current guidelines. *Proc. Natl. Acad. Sci. U.S.A.* **118**, e2105279118 (2021).
6. M. Jayaweera, H. Perera, B. Gunawardana, J. Manatunge, Transmission of COVID-19 virus by droplets and aerosols: A critical review on the unresolved dichotomy. *Environ. Res.* **188**, 109819 (2020).
7. S. Balachandar, S. Zaleski, A. Soldati, G. Ahmadi, L. Bourouiba, Host-to-host airborne transmission as a multiphase flow problem for science-based social distance guidelines. *Int. J. Multiph. Flow* **132**, 103439 (2020).
8. P. Azimi, Z. Keshavarz, J. G. Cedeno Laurent, B. Stephens, J. G. Allen, Mechanistic transmission modeling of COVID-19 on the *Diamond Princess* cruise ship demonstrates the importance of aerosol transmission. *Proc. Natl. Acad. Sci. U.S.A.* **118**, e2015482118 (2021).
9. J. M. Samet *et al.*, SARS-CoV-2 indoor air transmission is a threat that can be addressed with science. *Proc. Natl. Acad. Sci. U.S.A.* **118**, e2116155118 (2021).
10. L. Morawska, D. K. Milton, It is time to address airborne transmission of coronavirus disease 2019 (COVID-19). *Clin. Infect. Dis.* **71**, 2311–2313 (2020).
11. M. Abkarian, H. A. Stone, Stretching and break-up of saliva filaments during speech: A route for pathogen aerosolization and its potential mitigation. *Phys. Rev. Fluids* **5**, 102301 (2020).
12. M. Abkarian, S. Mendez, N. Xue, F. Yang, H. A. Stone, Speech can produce jet-like transport relevant to asymptomatic spreading of virus. *Proc. Natl. Acad. Sci. U.S.A.* **117**, 25237–25245 (2020).
13. M. Rodríguez-Hakim, L. Räz, J. Vermant, Variations in human saliva viscoelasticity affect aerosolization propensity. *Soft Matter* **18**, 2528–2540 (2022).
14. W. F. Wells, On air-borne infection*. Study II. Droplets and droplet nuclei. *Am. J. Epidemiol.* **20**, 611–618 (1934).
15. M. Alsved *et al.*, Exhaled respiratory particles during singing and talking. *Aerosol Sci. Technol.* **54**, 1245–1248 (2020).
16. S. Asadi *et al.*, Aerosol emission and superemission during human speech increase with voice loudness. *Sci. Rep.* **9**, 2348 (2019).
17. G. Johnson *et al.*, Modality of human expired aerosol size distributions. *J. Aerosol Sci.* **42**, 839–851 (2011).
18. X. Xie, Y. Li, H. Sun, L. Liu, Exhaled droplets due to talking and coughing. *J. R. Soc. Interface* **6** (suppl. 6), S703–S714 (2009).
19. Y. J. Hou *et al.*, SARS-CoV-2 reverse genetics reveals a variable infection gradient in the respiratory tract. *Cell* **182**, 429–446.e14 (2020).
20. S. Anand, Y. S. Mayya, Size distribution of virus laden droplets from expiratory ejecta of infected subjects. *Sci. Rep.* **10**, 21174 (2020).
21. R. R. Netz, Mechanisms of airborne infection via evaporating and sedimenting droplets produced by speaking. *J. Phys. Chem. B* **124**, 7093–7101 (2020).
22. R. R. Netz, W. A. Eaton, Physics of virus transmission by speaking droplets. *Proc. Natl. Acad. Sci. U.S.A.* **117**, 25209–25211 (2020).
23. C. Lieber, S. Melekidis, R. Koch, H. J. Bauer, Insights into the evaporation characteristics of saliva droplets and aerosols: Levitation experiments and numerical modeling. *J. Aerosol Sci.* **154**, 105760 (2021).
24. L. F. Pease, N. Wang, G. R. Kulkarni, J. E. Flaherty, C. A. Burns, A missing layer in COVID-19 studies: Transmission of enveloped viruses in mucus-rich droplets. *Int. Commun. Heat Mass Transf.* **131**, 105746 (2022).
25. E. P. Vejerano, L. C. Marr, Physico-chemical characteristics of evaporating respiratory fluid droplets. *J. R. Soc. Interface* **15**, 20170939 (2018).
26. D. H. Morris *et al.*, Mechanistic theory predicts the effects of temperature and humidity on inactivation of SARS-CoV-2 and other enveloped viruses. *eLife* **10**, e65902 (2021).
27. K. Lin, C. R. Schulte, L. C. Marr, Survival of MS2 and Φ6 viruses in droplets as a function of relative humidity, pH, and salt, protein, and surfactant concentrations. *PLoS One* **15**, e0243505 (2020).
28. A. Fedorenko, M. Grinberg, T. Orevi, N. Kashtan, Survival of the enveloped bacteriophage Phi6 (a surrogate for SARS-CoV-2) in evaporated saliva microdroplets deposited on glass surfaces. *Sci. Rep.* **10**, 22419 (2020).
29. H. P. Oswin *et al.*, Measuring stability of virus in aerosols under varying environmental conditions. *Aerosol Sci. Technol.* **55**, 1315–1320 (2021).
30. A. B. Acquier, A. K. D. C. Pita, L. Busch, G. A. Sánchez, Comparison of salivary levels of mucin and amylase and their relation with clinical parameters obtained from patients with aggressive and chronic periodontal disease. *J. Appl. Oral Sci.* **23**, 288–294 (2015).
31. A. Almstaahl, M. Wikström, Electrolytes in stimulated whole saliva in individuals with hyposalivation of different origins. *Arch. Oral Biol.* **48**, 337–344 (2003).
32. B. Larsson, G. Olivecrona, T. Ericson, Lipids in human saliva. *Arch. Oral Biol.* **41**, 105–110 (1996).
33. L. H. Schneyer, J. A. Young, C. A. Schneyer, Salivary secretion of electrolytes. *Physiol. Rev.* **52**, 720–777 (1972).
34. D. F. Evans, H. Wennerström, *The Colloidal Domain: Where Physics, Chemistry, Biology, and Technology Meet* (Wiley, 1999).
35. M. Rezaei, R. R. Netz, Airborne virus transmission via respiratory droplets: Effects of droplet evaporation and sedimentation. *Curr. Opin. Colloid Interface Sci.* **55**, 101471 (2021).
36. S. Basu, P. Kabi, S. Chaudhuri, A. Saha, Insights on drying and precipitation dynamics of respiratory droplets from the perspective of COVID-19. *Phys Fluids (1994)* **32**, 123317 (2020).
37. J. M. Andersson, K. Roger, M. Larsson, E. Sparr, The impact of nonequilibrium conditions in lung surfactant: Structure and composition gradients in multilamellar films. *ACS Cent. Sci.* **4**, 1315–1325 (2018).
38. K. Roger, M. Liebi, J. Heimdal, Q. D. Pham, E. Sparr, Controlling water evaporation through self-assembly. *Proc. Natl. Acad. Sci. U.S.A.* **113**, 10275–10280 (2016).
39. K. Roger, J. J. Crassous, How the interplay of molecular and colloidal scales controls drying of microgel dispersions. *Proc. Natl. Acad. Sci. U.S.A.* **118**, e2105530118 (2021).
40. N. Frossling, Uber Die Verdunstung Fallender Tropfen. *Beitr Geophys* **52**, 170–216 (1938).
41. B. Abramzon, W. A. Sirignano, Droplet vaporization model for spray combustion calculations. *Int. J. Heat Mass Transf.* **32**, 1605–1618 (1989).
42. K. Roger, E. Sparr, H. Wennerström, Evaporation, diffusion and self-assembly at drying interfaces. *Phys. Chem. Chem. Phys.* **20**, 10430–10438 (2018).
43. E. Huynh *et al.*, Evidence for a semisolid phase state of aerosols and droplets relevant to the airborne and surface survival of pathogens. *Proc. Natl. Acad. Sci. U.S.A.* **119**, e2109750119 (2022).
44. T. P. Peacock *et al.*, The SARS-CoV-2 variant, omicron, shows rapid replication in human primary nasal epithelial cultures and efficiently uses the endosomal route of entry. bioRxiv [Preprint] (2022). https://www.biorxiv.org/content/10.1101/2021.12.31.474653v1 (Accessed 15 February 2022).
45. S. Bourrous *et al.*, A performance evaluation and inter-laboratory comparison of community face coverings media in the context of COVID-19 pandemic. *Aerosol Air Qual. Res.* **21**, 200615 (2021).
46. I. A. Larmour, S. E. Bell, G. C. Saunders, Remarkably simple fabrication of superhydrophobic surfaces using electroless galvanic deposition. *Angew. Chem. Int. Ed. Engl.* **46**, 1710–1712 (2007).